

## Synthesis of Zinc oxide/reduced graphene oxide ( ZnO / rGO) nanocomposite to removal dyes from Aqueous solutions

**Baraa Ibrahim Abbas<sup>(1)</sup>**

Directorate of Education, Al\_Karkh the first, Ministry of Education<sup>(1)</sup>,

**Ali H. Alsadoon<sup>(2)</sup>,**

University of Babylon, collage of pharmacy<sup>(2)</sup>,  
Email [Alialsoud1987@gmail.com](mailto:Alialsoud1987@gmail.com)

**, Nada Abdulzahra Naet<sup>(3)</sup>**

Directorate of Education, Al\_Karkh the first, Ministry of Education<sup>(3)</sup>

**Halah Mohammed Azeez<sup>(4)</sup>,**

Medical Physics Department, Al-Mustaqbal University College, Iraq<sup>(4)</sup>,

**Nada Y.Fairooz<sup>(5)</sup>,**

University of Babylon, collage of science, dep. Of chemistry<sup>(5)</sup>,

**Gufran Hade seood<sup>(6)</sup>**

Al-Mustaqbal University Collage, dep.of Medical physics<sup>(6)</sup>

### ABSTRACT

Nanotechnology is the science that is used in different fields and different fields. And it has great value from the benefits that go into in the It benefits various technological and industrial sectors, including information technology, energy, medicine, and transportation environment and its safety from pollutants, food safety, and many other things, as well as working to adapt materials in Very small scales have properties of active substances, and from these properties they are more durable and intertwine. In this work, the environmental aspect was applied and used, and the developers saw a need to develop nanocomposites to remove dyes from aqueous solutions to reduce environmental and health damage. Therefore, methods of synthesis of nanomaterials were developed in many different ways and in an increasing state. And the possibility of manipulating the chemical and physical properties by changing the particle size and using it in many of the above-mentioned applications and one of these applications is adsorption as in this work. To work on the adsorption property, the RGO nanoparticles were synthesized by the hydrothermal method and doped with zinc oxide (ZnO) nanoparticles that were also synthesized by the hydrothermyl method to produce (ZnO / RGO) nanocomposites and their properties were studied. The samples were examined with multiple analytical techniques such as X-ray diffraction (XRD), field emission scanning electron microscopy (FE-SEM), and energy dispersive X-ray analysis (EDX) to study their structure, morphology and thermal stability. And the identification of the reaction mechanism and the efficiency of absorption of rhodamine dye on this nanocomposite. Depending on different absorption conditions such as effect of temperature, mass dose of materials used, contact time and pH.

**Keywords:**

Zinc oxide , water pollution, nanomaterials

## 1. Introduction

Industrial dyestuffs and textile dyes are among the most dangerous organic chemicals, according to the paper. According to a World Bank estimate, textile finishing and dyeing industries are responsible for nearly 17–20 percent of water pollution. According to a Kant study, 72 of the primary identified wastewater hazardous compounds were generated simply by textile dyeing, and approximately 30 of these pollutants were untreatable [1]. Due to its wide band gap (3.37 eV) and high exciton binding energy, zinc oxide (ZnO) has received significant attention for applications in nanoscale electrical and optoelectronic devices (60 meV) [2]. The fact that ZnO is a polar crystal with a hexagonal phase and exhibits high anisotropy causes its growth to be oriented along the *c* axis is also widely known [3]. ZnO is a good replacement for TiO<sub>2</sub> in terms of band energy [4]. Zinc oxide (ZnO) nanoparticles are materials with numerous industrial uses, such as fluorescent tube luminescence material, laser active medium, sensors, and antimicrobial agents [5–7]. As a result, the researcher is quite interested in the synthesis of ZnO nanoparticles. Sol-gel, sonochemical, solvothermal, hydrothermal, and mechanochemical methods are some of the chemical techniques that have been used to create ZnO nanoparticles [8]. Graphene has a unique two-dimensional structure with the thickness of an atom, and excellent mechanical, optical, thermal, and electronic properties [9]. As a result, numerous applications in electronics [10], catalysis [11], sensors [12], energy conversion and storage [13, 14], etc., have been investigated. For these goals, the mass manufacture of graphene materials at affordable costs is one of the basic requirements. In fact, graphene has a two-dimensional (2D) structure of sp<sup>2</sup> hybrid carbon atoms, so it possesses unique properties such as high surface area, absorption and good electrical conductivity. Even rGO, after forming the compound with semiconductors, also possesses the ability to accept photogenic electrons to prevent recombination and provides adequate adsorption of the dye through coupling ( $\pi - \pi$ ) between the dye and the surface of the rGO [15]. Due to graphene's

ability to transfer ballistic electrons, it can effectively demonstrate In a rich structure, there is zero conduction resistance for storing and moving electrons. Thus, these compounds naturally shorten the time needed for the electron-hole pair to recombine, improving the photocatalytic capability for the destruction of harmful dyes [16, 17]. Zhang and colleagues synthesized ZnO / rGO compounds for photodegradation of Rh6G under ultraviolet light irradiation [18]. To create a (ZnO-RGO) hybrid, Many techniques have been used. By binding ZnO nanoparticles to GO and reducing GO to RGO via hydrothermal treatment with ethanol, ZnO nanoparticles were bound to RGO. [19]. Here, we report the ease with which nanocomposites were synthesized By synthesizing graphene oxide (GO) from graphite powder In a modified Hummer fashion. And combine them to produce (ZnO / rGO) nanocomposite by Hydrothermal method using zinc chloride under the influence of ultrasonic. (ZnO / rGO) was used as an application in removing dyes from aqueous solutions by means of Its adsorption to rhodamine (Rh-6G) dye.

## 2. Experimental.

### 2.1- Materials and Chemicals.

All of the precursors, including sodium nitrate (NaNO<sub>3</sub>) with a 99.5 percent assay, potassium permanganate (KMnO<sub>4</sub>) with a 99.5 percent assay, zinc acetate dihydrate (Zn(CH<sub>3</sub>COO)<sub>2</sub>H<sub>2</sub>O) with a 98.5 percent assay, sulfuric acid (H<sub>2</sub>SO<sub>4</sub>) with a 98 percent assay, and other chemicals with an AR grade, were imported from SRL, India. Graphite powder with a purity of 99 percent was offered by Sigma-Aldrich. powdered rhodamine dye from Sigma Aldrich. For the synthesis, deionized water (DI water) was used.

### 2.2 Synthesis of Reduced Graphene Oxide (rGO).

The graphite powder was oxidized using a modified Hummer's technique [20]. In an ice bath, a combination of pre-oxidized graphite (3 g), Na NO<sub>3</sub> (1.5 g), and H<sub>2</sub>SO<sub>4</sub> (115 mL) is

agitated for 20 minutes. Then, slowly add  $\text{KMnO}_4$  (9 g) to the suspension while stirring vigorously and maintaining a constant temperature ( $>20^\circ\text{C}$ ). The temperature of the solution was then raised to  $35^\circ\text{C}$  and agitated continuously for nearly 12 hours. 300 mL DI water was added after the temperature of the precursor solution was raised to  $98^\circ\text{C}$ . The residual manganese dioxide and permanganate were then removed from the suspension using 30 weight percent colorless  $\text{H}_2\text{O}_2$  after it had been diluted with 1 L DI water. The pH of the mixture was neutralized by filtering and washing with 5 weight percent  $\text{HCl}$  aqueous solution and DD water, respectively. The mixture was then vacuum-dried for 24 hours at 40 degrees Celsius to produce the finished form of GO. The obtained GO was combined with the reducing agent (Thiourea) at  $100^\circ\text{C}$  for roughly 24 hours with constant stirring, yielding rGO [21].

### 2.3 Synthesis of ZnO Nanoparticles.

First, 20 mL of dimethyl sulfoxide (DMSO) was used to dissolve 0.2 M zinc acetate dihydrate ( $\text{Zn}(\text{CH}_3\text{COO})_2 \cdot 2\text{H}_2\text{O}$ ), and then 20 mL of ethanol was used to dissolve 1.2 M potassium hydroxide (KOH). The  $\text{Zn}(\text{CH}_3\text{COO})_2 \cdot 2\text{H}_2\text{O}$  solution is then gradually mixed with KOH solution until it turns milky white. Under constant stirring, 0.2 mL of tri-ethanolamine (TEA) was added to the milky solution as a capping agent. After that, the precipitate was centrifuged to separate it from the liquid. After being washed three times, the precipitate was dried at  $90^\circ\text{C}$  to produce a fine white powder. The sample was then used for further analysis after being annealed at 400 degrees Celsius [21].

### 2.4 Formation of rGO/ZnO Nanocomposite.

The rGO/ZnO nanocomposite was made using a simple ultrasonic-assisted solution technique. 1 g of rGO was sonicated for 30 minutes with 150 mL DI water. Similarly, 0.25 g of ZnO was mixed with 50 mL DI water and sonicated for 30 minutes separately. Both solutions were then combined and sonicated for 45 minutes before being agitated constantly for 1 hour and dried in a hot air oven. The rGO/ZnO nanocomposite powder was finally obtained [21].

### 2.4. Adsorption experiments.

#### 2.4.1. Batch adsorption experiments

The stock solution of 50 mg/L Rh.6G solution was prepared by dissolving 0.05 g of Rh.6G powder in 100 mL of water. An aqueous solution (10 mL) with 0.1 g ( $\text{ZnO}$  / rGO) nanocomposite and a suitable concentration of Rh.6G was shaken by a thermostatic reciprocating shaker at 120 rpm at 297K. After removal of the nanocomposite by filtration through a centrifuge of 6,000 rpm, the dye concentrations in the supernatant were determined by a UV-Visible spectrophotometer. The amount of ( $\text{ZnO}$  / rGO) adsorbed by adsorbent ( $q$ ) in the adsorption systems were calculated by the following mass balance Eq.(1) :

$$q = \frac{V \cdot (C_0 - C_e)}{m}$$

(1)

and the percent removal (%) of ( $\text{ZnO}$ -RGO) was calculated using the following Eq. (2) :

$$\text{removal \%} = \frac{(C_0 - C_e)}{C_0} \times 100\%$$

(2)

where  $C_i$  and  $C_e$  (mg/l) are the starting and equilibrium metal concentrations in the water, respectively, and  $V$  is the volume of the solution (l),  $m$  is the weight of the adsorbent (g), and [22].

#### 2.4.2. Effect of adsorbent dosage.

Effect of surface mass ( $\text{ZnO}$  / rGO) on a process The absorption of dyes was studied with different weights (0.001, 0.006, 0.02, 0.07, 0.1 g). For every 10 ml of dye solution, the dye was mixed in a solution with an adsorbed surface it is placed in a water bath shaker for 6 hours. Then the samples were expelled at 6000 rpm for adsorbent removal. Here all conditions are required to be stable. Dye concentration, temperature, and acidic function). Then the remaining dye concentration is measured with (UV-Vis) Spectrophotometer.

#### 2.4.3. Temperature effect.

In this agent adsorption was carried out in the same way and a variable range of concentrations between (1-12) mg / liter was used to estimate the basic thermodynamic functions at temperatures (10 ° C, 15 ° C, 20 ° C, 25 ° C, and 30 ° C).

**2.4.4. Effect of pH**

The effect of acidity on adsorption has been studied Process. To measure the pH we used a pH scale .At the beginning of the adsorption, different pH values ranging between (2.0--12.0) were taken to regulate the pH With a solution of HCl and NaOH diluted (0.1 M). All conditions are at temperature 25 ° C and a concentration of( 10 mg / L). Weight (0.1g) For nanocomposite (ZnO / rGO) and dye solutions.and we plotted the results The amount absorbed versus a value The acidic function and its effect on the adsorption process.

**3. Results and discussion**

**3.1. Characterization.**

**3.1.1XRD of reduce Graphen Oxide (rGO) and Zinck Oxide (ZnO) nanoparticales and (ZnO / rGO) nanocomposite.**

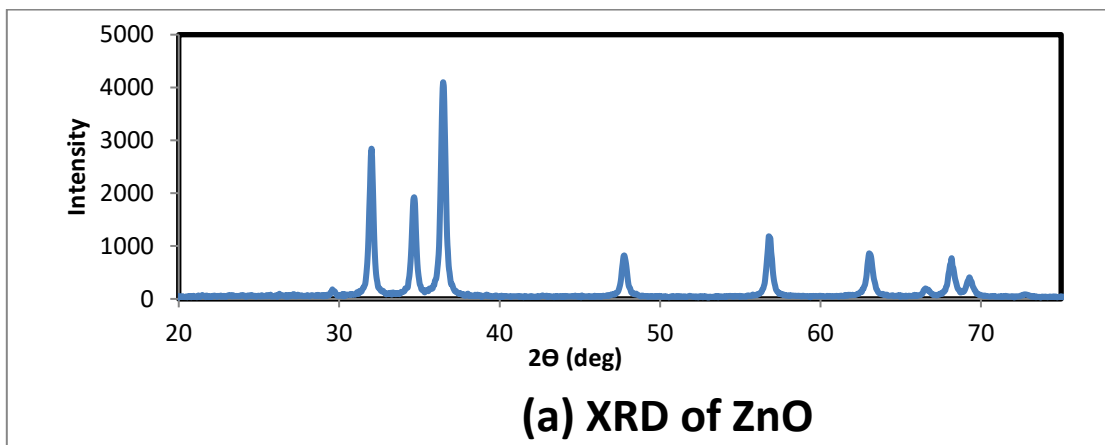
The average size of the crystallites was estimated from the broadening of thehighest diffraction peak, using the Scherrer equation [23]. The crystallite size using the Debby-Scherrer Eq.(3) .

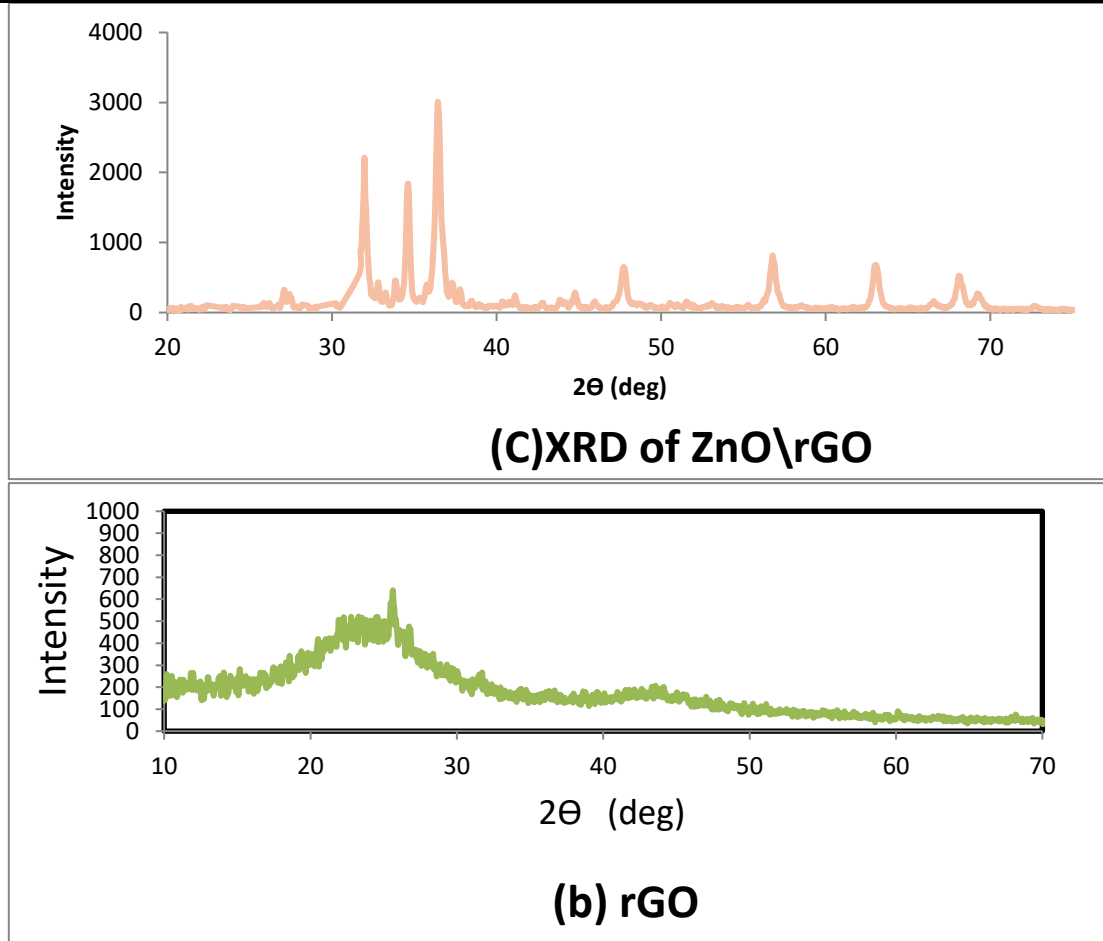
$$D = \frac{K \lambda}{\beta \cos \theta} \dots\dots\dots (3)$$

where  $\beta$  is a half width of the peak , D is the crystalline size in nanometers (nm), k is a constant equal to 0.9 and  $\lambda=1.5406 \text{ \AA}$  is the wavelength of CuK $\alpha$  radiation.

The interplanar distance (d) and the lattice constants (a, c) were calculated using the relation  $2d\sin\theta = n\lambda$  and  $1/d^2 = [(4/3)\{ ((h^2 + hk + k^2 )/a^2 ) \} + ( 1/2c^2 ) ]$  [24].

Figure.1 presents the results of X-ray diffraction for the ZnO-NPs after synthesis showing wide peaks at position ( 31.9, 34.6, 36.47.7 , 56.7 and 68.1) characteristic to the ZnO structure. and show Fig.(1.a) the number of strong diffraction peaks (JCPDS Card numbers 008, 82-1042, and 5-0664) that correspond to the 100, 002, 101, 102, 110, 103, 112, and 201 reflection lines of the hexagonal wurtzite structure of zinc oxide nanoparticles [25]. measured were about (19.5 nm , 26.6 nm, 16.8 nm, 17.4 nm , and 14.6 nm and 13.9 nm). Fig. (1.b) shows the XRD pattern of reduced graphene oxide Following the thermochemical treatment, the reduction of rGO was confirmed by diffraction peak that appeared at  $2\theta=26.8^\circ$  , reflection plane (002) [26].and nanoscale (23.96 nm) and nanoscale (23.96 nm). The XRD spectrum of the ZnO / rGO complex is shown in Fig. (1.b) the hexagonal ZnO reflection. The peaks were more dominant, (JCPDS file no. 01-089-0510). There are no other reflection peaks, including (001) rGO Reflections and may indicate the formation of high-purity ZnO. Absence of a graphen oxide reflection peak (002) at Peack ( 25.6) indicates that the surface of the rGO is completely covered With ZnO nanoparticles [27]. The size of the nanoparticles was (23.9nm).





**3.1.2 EDX - analysis.**

was used to examine the purity of the compound ZnO NPs, Fig. (2.a) EDX indicates that the Zn and O elements Zn content was 81.2% while the O content was 12.0 %. He indicated that the ZnO NPs were pure with only few impurities. The single peak of Zn and O is between 0 and 2. There are two zinc peaks between 8 and 10. These results coincide with results already reported with the same results The peak site in

the synthesis of zinc oxide. . Also, the appearance of high carbon in EDX in Fig. (2.b) which is (65.6, 33.1%) and second peak is attributable to the oxygen present in rGO. As for Fig. (2.c) it shows the EDX image, and the emergence of pccs whose proportions (64.1, 21.6 and 12.0%) are due to Zn, O and C, respectively, with the presence of some impurities, as mentioned previously

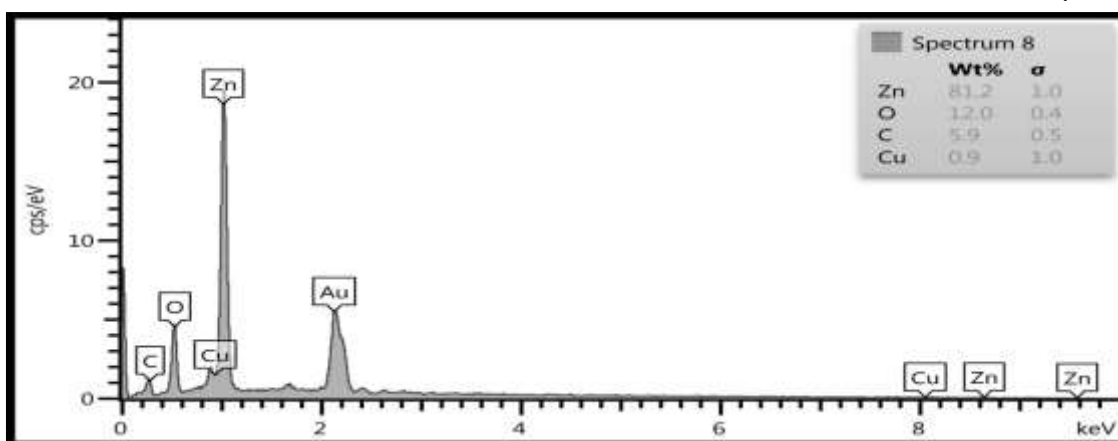


Fig.(2) show EDX of (a) ZnO

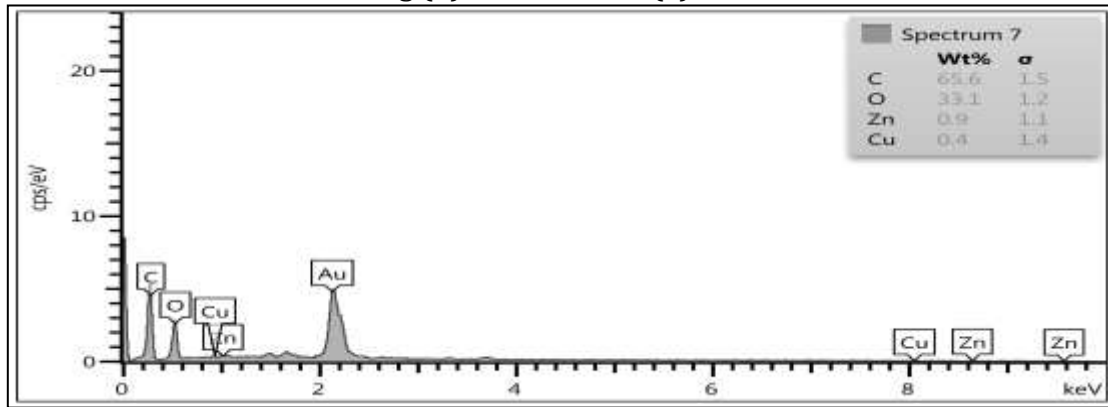


Fig.(2) show EDX of (b) rGO

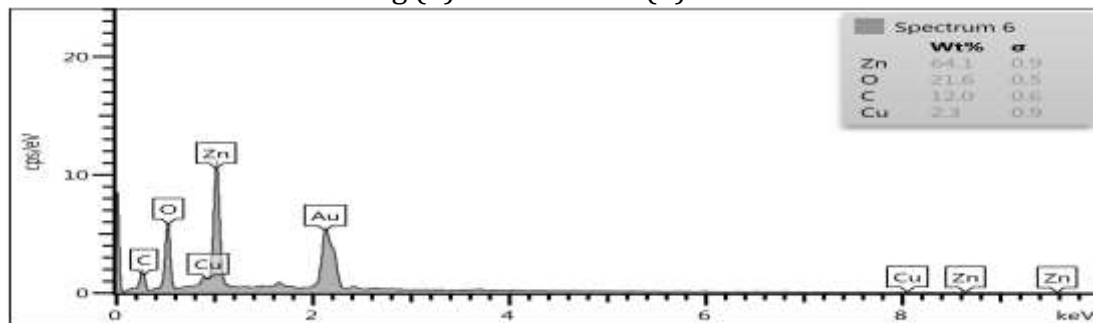


Fig.(3) show EDX of (C) ZnO\rGO

**3.1.3 FE-SEM analysis.**

In Figure 6, a set of FESEM images of the nanocomposite formation stages (Fig.3a) shows the FE-SEM image of the rGO. We observed the formation of micro / nanostructures as arranged sheets. (Fig. 3b) The FESEM image of ZnO exhibits the formation of densely arranged (Fig. 3c) shows ) spherical-shaped structures.

an image showing a FESEM image of the ( ZnO / rGO nanocomposite of a group of pellets spread along the plates, indicating the formation of the nanocomposite assembled using both zinc pellets and reduced graphene oxide plates.

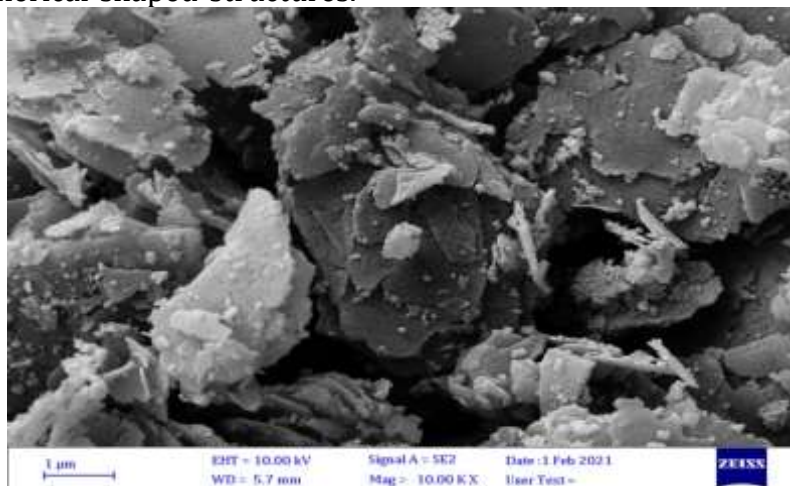


Fig.(3) (a) show FESEM of rGO

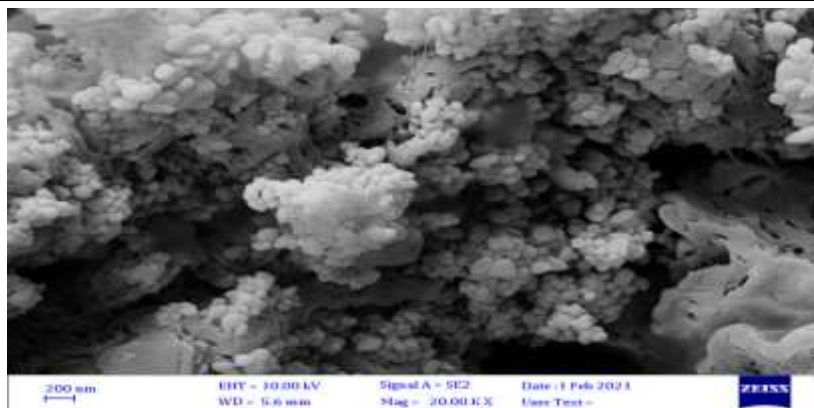


Fig.(3) (b) show FESEM of ZnO

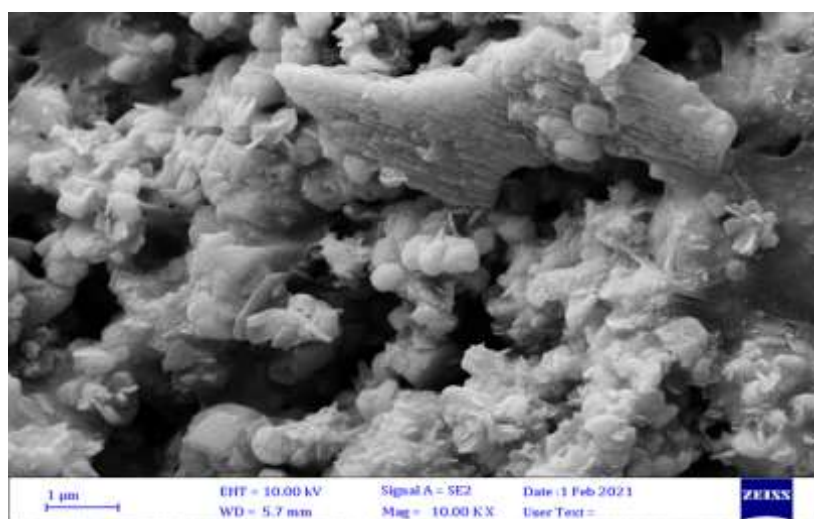


Fig.(3) (c) show FESEM of ZnO\ rGO

### 3.1.4 The FTIR spectrum.

The FTIR spectrum is shown in Figure 6. For ZnO, rGO and ZnO-rGO nanoparticles. (Fig. 4 a) refers to ZnO synthesized by the hydrothermal method. We observed the emergence of a peak confined between (400-4000  $\text{cm}^{-1}$ ) of the spectrum, there are two peaks near (597.95  $\text{cm}^{-1}$  and 486.08  $\text{cm}^{-1}$ ) due to the vibration of the bundle (Zn- O). There are other peaks confined between (600-2000  $\text{cm}^{-1}$ ) that may be vibration of bonds (c-c, c = c, co<sub>2</sub>) for the acetate group due to the carboxylic acid. A peak near of (3100 and 3600  $\text{cm}^{-1}$ ) is due to the C-H expansion[28].

(Fig. 4 b) shows the FTIR spectra of reduced graphene oxide (rGO), the figure shows the presence of sporadic modified peaks between (3200-3800  $\text{cm}^{-1}$ ), the presence of an OH bond due to the hydroxyl group in (rGO). -1,430  $\text{cm}^{-1}$

1) of wavelength due to vibration of bonds (C = O, (-COOH group), COC (epoxy group) [29].

(Fig. 4 c) shows the FTIR spectra of the ( ZnO / r GO ) nanocomposite. We noticed that the broad peaks in the FTIR spectra centered between (400-2000  $\text{cm}^{-1}$ ) which are (518.87  $\text{cm}^{-1}$  420.50 and  $\text{cm}^{-1}$ ) and belong to Zn-O, and there are other peaks resulting from the expansion of O - H and C-H bonds. The C-OH, c-c, c = c, co<sub>2</sub> and the C-O stretching respectively returning to rGO were significantly decreased. As well as the summits confined between (3100 -3800  $\text{cm}^{-1}$ ) of the spectrum region and the resulting vibration of the O - H and C-H bonds were also decreased. Denotes the formation of the ZnO / r GO nanocomposite obtained from ZnO NPs decorated on RGO sheets.

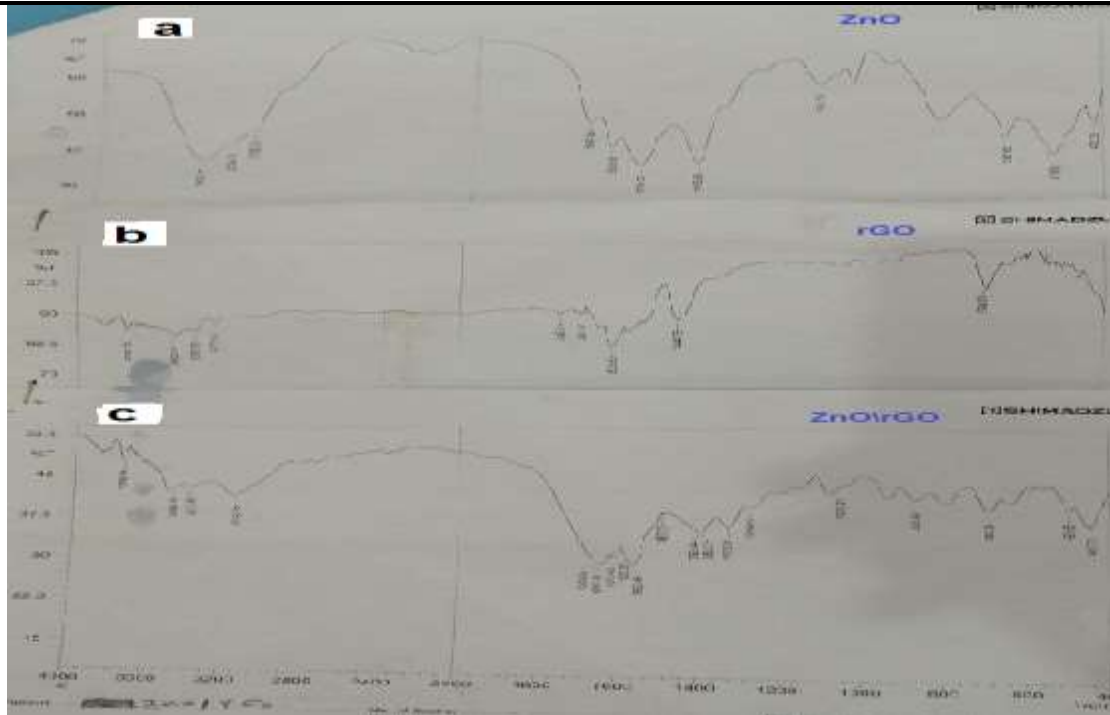


Fig.(4) show the FTIR-for (a)ZnO (b)rGO (c) ZnO\rGO

### 3.2 Adsorption experiments.

#### 3.2.1.Effect of adsorbent dosage .

An experiment with adsorption to remove rhodamine 6G dye, It was performed using different weights (0.001 - 0.1 g) of the nanocomposite. Note that as the weight of the nanocomposite increases, the dye will increase the removal rate. Attributed to the larger surface area of the nanocomposite and An increase in the active sites available for uptake of the Rh.6G dye Thus, the Rh.6G uptake reaches the of nanocomposites as surface active sites From rGO / Co3O4 it becomes saturation level at 0.1g saturated with Rh.6G. Later For experiments, 0.1 g was selected from the sorbent dose (Fig 5) [30].

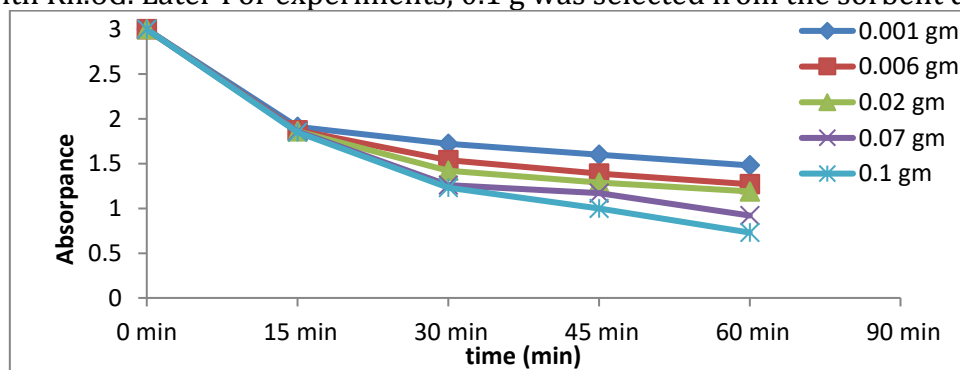


Fig.( 5) the Effect of dosage

#### 3.2.2.The effect of contact time .

The adsorption dye has been studied at various times. (1-75 minutes) after stabilizing for all influencing conditions .In Rhodamine 6G the dye absorption capacity was increased .With increasing (time to its maximum value saturation state) but sometimes the adsorption capacity decreases with Increased time due to the absorption process [31].

#### 3.2.3.Effect of pH .

An important factor influencing the dye adsorption process is the solution pH. By changing the surface charge of the adsorbent and the ionization behavior of the adsorbent and dye.

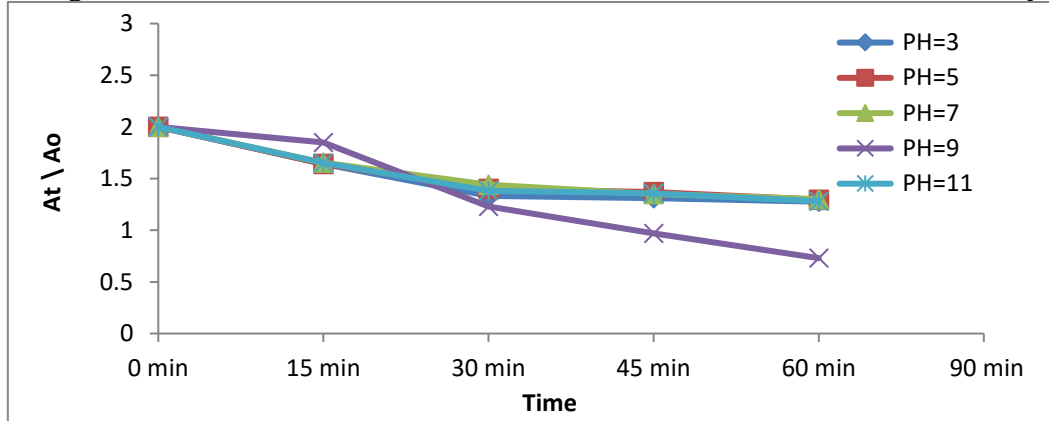


Fig. ( 6) the effect of the pH

In (Fig. 6) show the effect of the pH on the solution is shown. Removing Rh.6G by ZnO / rGO, it is possible. It should be noted that the dye removal efficiencies by the nanocomposite increase with increasing pH in the pH range from 2.0 to 12.0. The decrease in the adsorption capacity is observed at a low pH value. Attributed to the competition of protons with cation. Rh.6G for adsorption sites available on the ZnO \ rGO surface. Electrostatic attraction between the two negatives. A charged ZnO \ rGO and Rh.6G cation will lead to increase the adsorption capacity [32].

### 3.3. Adsorption isotherms and Adsorption kinetic :

To match the experimental adsorption data for Rh6G on ZnOrGO, the adsorption isotherm Langmuir and Freundlich models were applied. The adsorption isotherm Langmuir model is commonly accepted for describing molecule adsorption on homogeneous surfaces, while the adsorption Freundlich model is utilized to explain heterogeneous systems as surfaces with non-energetically equal sites. Eq.(4)(5) [33] The linear equations of the Langmuir and Freundlich isotherms can be expressed as follows:

$$.....(4) \frac{ce}{q_e} = \frac{1}{q_m \cdot b} + \frac{ce}{q_m}$$

$$\log q_e = \log K_F + 1/n \log C_e .....(5)$$

q<sub>e</sub> is the equilibrium adsorption value (mg g<sup>-1</sup>), and C<sub>e</sub> is the RhB equilibrium concentration

(mg l<sup>-1</sup>). The theoretical maximum adsorption capacity (mg g<sup>-1</sup>) is given by q<sub>m</sub>. Freundlich and Langmuir constants are K<sub>f</sub> and b, respectively. The heterogeneity factor, or 1/n, is a measure of adsorption efficiency. Were employed two types of Pseudo-first order and pseudo-second order kinetics models are examples of kinetic models. to look into adsorption rate for adsorption process of Rh6G on the prepared nanomaterials in the present study. The pseudo-first order model also known Lagergren equation there liner form can be expressed as Eq.(6) [33].

$$.....(6) \ln(q_t - q_e) = \ln(q_e) - k_1 t$$

Where: q<sub>e</sub> and q<sub>t</sub> (mg/g) are the amounts of the Rh6G adsorbed at equilibrium and at time t (min), respectively, k<sub>1</sub> (min<sup>-1</sup>) the adsorption rate constant, slope = -K<sub>1</sub>, and intercept = log q<sub>e</sub>. Pseudo-second order model there liner form can be expressed as Eq.(7) [33]

$$.....(7) \frac{t}{q_t} = \frac{1}{k_2 q_e^2} + \frac{t}{q_e}$$

Where: k<sub>2</sub> (L.mol<sup>-1</sup>. min<sup>-1</sup>) is the rate constant of the second order equation (g/mg min). When plotting between t/q<sub>t</sub> and t, slope = 1/q<sub>e</sub> and intercept = 1/K<sub>2</sub>q<sub>e</sub><sup>2</sup>. After we have applied the adsorption values in the Langmuir and Freundlich equations we can determine that the Langmuir isotherms are connected to the comparable adsorption energies and monolayer adsorption at homogeneous locations, whereas Freundlich described for heterogeneous surfaces [34].

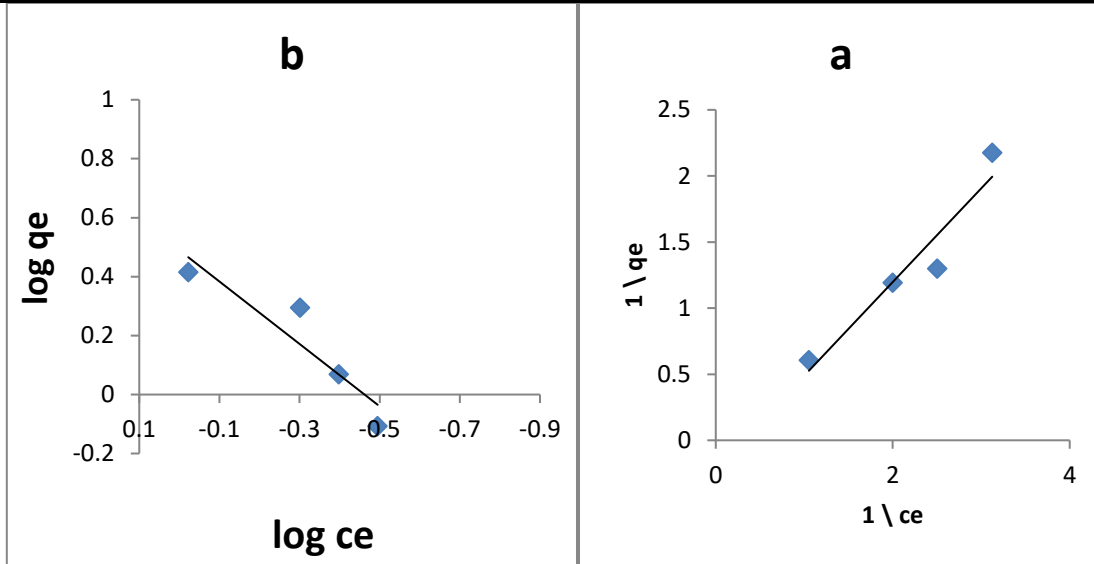


Fig. (7) shows (a) Langmuir adsorption isotherm (b) Freundlich adsorption isotherm

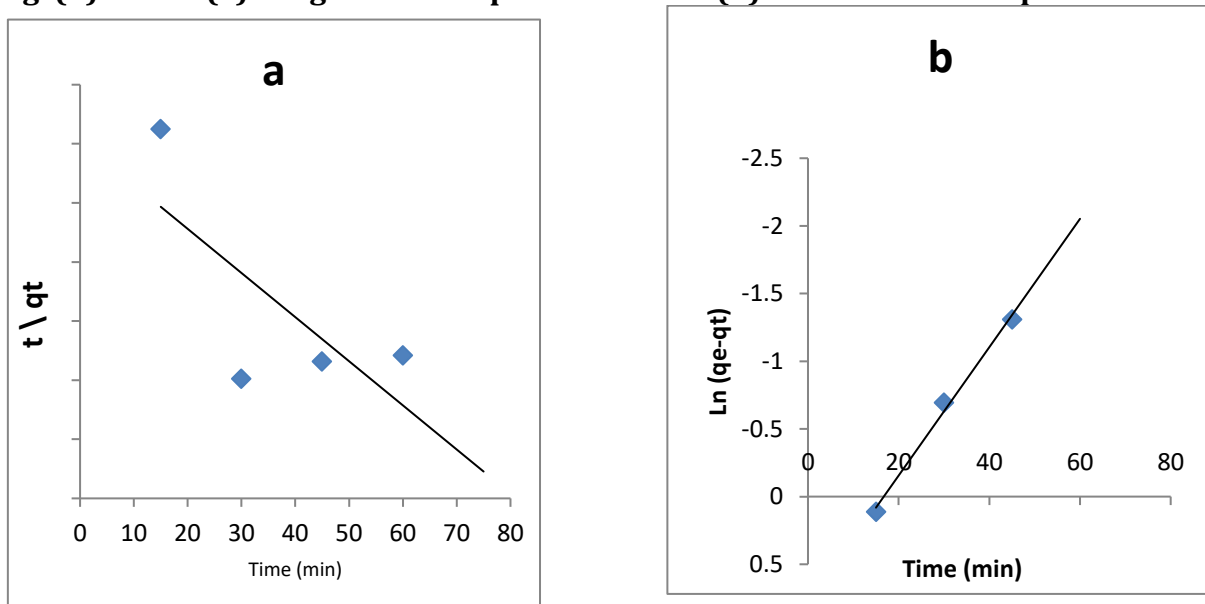


Fig. (8) shows of kinetics model (a) pseudo-second-order(b) pseudo-first- order

And after we applied the adsorption values in the equations of Langmuir and Freundlich gave us the Fig. (7. a, b), we can decide that it is a more suitable Langmuir model. On the other hand, the correlation coefficient ( $R^2$ ) for Freundlich (0.8572) is relatively smaller than that of Langmuir (0.9183). Therefore, the adsorption of the dye on the surface of the nanocomposite occurred well, as did the

shape. Fig. (8.a, b) It was well suited to the pseudo-first order kinematics model, to arbitrate in as well as the correlation coefficient having values (0.9820 and 0.9630) for the first and second order pseudo-kinematics respectively.

Table (1): Freundlich and Langmuir parameters for adsorption of Rh6G.

Isotherms	parameters	Values
-----------	------------	--------

Langmuir	$K_L$	6.428196
	$q_m$	4.5537341
	$R^2$	0.9183
Freundlich	$K_F$	3.086029
	$n$	0.4894
	$R^2$	0.8572

**Table 2**  
Adsorption kinetics parameters of adsorption of Rh.6G.

Pseudo first order model				
	$q_{e,exp}$ (mg/g)	$q_{e,cal}$ (mg/g)	$K_1$ ( $\text{min}^{-1}$ )	$R^2$
1	1.24	2.2098	1265.82	0.9941
Pseudo second order model				
	$q_{e,exp}$ (mg/g)	$q_{e,cal}$ (mg/g)	$K_2$ (g/mg.min)	$R^2$
2	1.24	0.6697027	0.0037042	0.5204

### Conclusion:

In this work, ZnO and rGO nanoparticles were successfully prepared and ZnO loaded onto rGO by the hydrothermal method to produce a ZnO / rGO nanocomposite. It was also found that the rGO / ZnO nanocomposite has great potential as an effective Rh.6G removal agent from aqueous solution. Adsorption process: corresponds to a typical pseudo-second class adsorption process. The isothermal model fit the Langmuir isothermal model and was part of the chemical adsorption process. Moreover, the pH value had a significant effect on the absorption capacity, and the adsorption of Rh 6G stain by the ZnO / rGO nanocomposite When the pH was raised, it first climbed and then declined dramatically.

### References:

1. Ajmal, Anila, et al. "Principles and mechanisms of photocatalytic dye degradation on TiO<sub>2</sub> based photocatalysts: a comparative overview." *Rsc Advances* 4.70 (2014): 37003-37026.
2. Ü. Özgür, Ya.I. Alivov, C. Liu, A. Teke, M.A. Reshchikov, S. Doğan, V. Avrutin, S.J. Cho, H. Morkoç, A comprehensive review of ZnO materials and devices, *Journal of Applied Physics* 98 (2005) 041301.
3. Q. Wu, X. Chen, P. Zhang, Y. Han, X. Chen, Y. Yan, S. Li, Amino acidassisted synthesis of ZnO hierarchical architectures and their novel photocatalytic activities, *Crystal Growth and Design* 8 (2008) 3010–3018.
4. J. Tian, Q. Zhang, L. Zhang, R. Gao, L. Shen, Sh. Zhang, X. Qu, G. Cao, ZnO/TiO<sub>2</sub>nanocable structured photoelectrodes for CdS/CdSe quantum dot co-sensitized solar cells, *Nanoscale* 5 (2013) 936–943.
5. Talam S, Srivinasa RK, Nagarjuna G. Synthesis, characterization, and spectroscopic properties of ZnO nanoparticles. *IRSN Nanotechnol* 2012:1–6.
6. Rajendran R, Balakumar. C, Hasabo AMA, Jayakumar S, Vaideki K, Rajesh EM. Use

- of zinc oxide nano particles for production of antimicrobial textiles. *Int J Eng Sci Technol* 2010;2(1):202–8.
7. Rai P, Yeon TY. Citrate-assisted hydrothermal synthesis of single crystalline ZnO NPs for gas sensor application. *Sens Actuators B: Chem* 2012.
  8. Aneesh PMK, A Vanoja M, Jayaraj K. Synthesis of ZnO nanoparticles by hydrothermal method. *Nanophotonic Mater IV* 2007:6639.
  9. Novoselov KS, Fal'ko VI, Colombo L, Gellert PR, Schwab MG, Kim K. A roadmap for graphene. *Nature* 2012;490(7419):192–200.
  10. Weiss NO, Zhou H, Liao L, Liu Y, Jiang S, Huang Y, et al. Graphene: an emerging electronic material. *Adv Mater* 2012;24(43):5782–825.
  11. Huang C, Li C, Shi G. Graphene based catalysts. *Energy Environ Sci* 2012;5(10):8848–68.
  12. Liu Y, Dong X, Chen P. Biological and chemical sensors based on graphene materials. *Chem Soc Rev* 2012;41(6):2283–307.
  13. Sun Y, Wu Q, Shi G. Graphene based new energy materials. *Energy Environ Sci* 2011;4(4):1113–32.
  14. Wassei JK, Kaner RB. Oh, the places you'll go with graphene. *Acc Chem Res* 2013.
  15. K.S. Kim, Y. Zhao, H. Jang, S.Y. Lee, J.M. Kim, K.S. Kim, J.H. Ahn, P. Kim, J.Y. Choi, B.H. Hong, Large-scale pattern growth of graphene films for stretchable transparent electrodes, *Nature Letters* 457 (2009) 706–710.
  16. B. Wang, W. Feng, L. Zhang, Y. Zhang, X. Huang, Z. Fang, P. Liu, In situ construction of a novel Bi/CdS nanocomposite with enhanced visible light photocatalytic performance, *Appl. Catal. B Environ.* 206 (2017) 510–519.
  17. S. Mahalingam, Y.H. Ahn, Improved visible light photocatalytic activity of rGOFe<sub>3</sub>O<sub>4</sub>-NiO hybrid nanocomposites synthesized by in-situ facile method for industrial wastewater treatment applications, *New J. Chem.* 42 (2018) 4372–4383
  18. C. Zhang, J. Zhang, Y. Su, M. Xu, Z. Yang, Y. Zhang, Hydrothermal preparation of ZnO-reduced graphene oxide hybrid with high performance in photocatalytic degradation, *Physica* 56 (2014) 251–255.
  19. B.J. Li, H.Q. Cao, ZnO@graphene composite with enhanced performance for the removal of dye from water, *J. Mater. Chem.* 21 (2011) 3346–3349.
  20. Zaaba, N. I., et al. "Synthesis of graphene oxide using modified hummers method: solvent influence." *Procedia engineering* 184 (2017): 469-477.
  21. Jayachandiran, J., et al. "Synthesis and electrochemical studies of rGO/ZnO nanocomposite for supercapacitor application." *Journal of Inorganic and Organometallic Polymers and Materials* 28.5 (2018): 2046-2055.
  22. Hossain, M. A., et al. "Removal of copper from water by adsorption onto banana peel as bioadsorbent." *International Journal of Geomate* 2.2 (2012): 227-234..
  23. Afqir, Mohamed, et al. "Morphology Control of SrBi<sub>2</sub>Nb<sub>2</sub>O<sub>9</sub> Prepared by a Modified Chemical Method." *Science of Sintering* 51.4 (2019).
  24. [24] Kumaresan, N., and K. Ramamurthi. "Synthesis of ZnO/rGO nanocomposites by wet impregnation method for photocatalytic performance against RhB dye and 4-chlorophenol under UV light irradiation." *Journal of Materials Science: Materials in Electronics* 31.4 (2020): 3361-3374.
  25. [25] Shamim, Aisha, Monis Bin Abid, and Tariq Mahmood. "Biogenic synthesis of zinc oxide (ZnO) nanoparticles using a fungus (*Aspergillus niger*) and Their Characterization." *International Journal of Chemistry* 11.2 (2019): 119-126.
  26. [26] Soomro, Sumair A., et al. "Improved performance of CuFe<sub>2</sub>O<sub>4</sub>/rGO nanohybrid as an anode material for lithium-ion batteries prepared via facile one-step method." *Current Nanoscience* 15.4 (2019): 420-429.

27. [27] Raja, Mohan, et al. "Studies on electrochemical properties of ZnO/rGO nanocomposites as electrode materials for supercapacitors." *Fullerenes, Nanotubes and Carbon Nanostructures* 23.8 (2015): 691-694.
28. [28] Manoj, V., et al. "Synthesis of ZnO nanoparticles using carboxymethyl cellulose hydrogel." *Asian J. Appl. Sci* 7.8 (2014): 798-803.
29. [29] Hidayah, N. M. S., et al. "Comparison on graphite, graphene oxide and reduced graphene oxide: Synthesis and characterization." *AIP Conference Proceedings*. Vol. 1892. No. 1. AIP Publishing LLC, 2017.
30. [30] P. Banerjee, P. Das, A. Zaman, P. Das, Application of graphene oxide nanoplatelets for adsorption of ibuprofen from aqueous solutions: evaluation of process kinetics and thermodynamics *Process Saf. Environ. Prot.*, 101 (2016) 45–53.
31. [31] G. Sharma, M. Naushad, A.H. Al-Muhtaseb, A. Kumar, M.R. Khan, S. Kalia, Shweta, M. Bala, A. Sharma, Fabrication and characterization of chitosan-crosslinked-poly(alginic acid) nanohydrogel for adsorptive removal of Cr(VI) metal ion from aqueous medium, *Int. J. Biol. Macromol.*, 95 (2017): 484–493.
32. [32] H.B. Senturk, D. Ozdes, C. Duran, Biosorption of Rhodamine 6G from aqueous solutions onto almond shell (*Prunus dulcis*) as a low cost biosorbents, *Desalination*, 252 (2010): 81–87.
33. [33] Sadeek, Sadeek A., et al. "Metal adsorption by agricultural biosorbents: adsorption isotherm, kinetic and biosorbents chemical structures." *International journal of biological macromolecules* 81 (2015): 400-409.
34. [34] Ramadan, Rania, and Seham K. Abdel-Aal. "Facile Synthesis of Nanostructured ZnO-rGO Based Graphene and Its Application in Waste Water Treatment." (2